Available online at www.derpharmachemica.com

ISSN 0975-413X
CODEN (USA): PCHHAX

Der Pharma Chemica, 2017, 9(13):19-31
(http://www.derpharmachemica.com/archive.html)

Quantum Computational and Vibrational Spectroscopic Analysis on N-((1-(phenylsulfonyl)-3-(phenylthio)-1H-indol-2-yl)methyl)acetamide

Srinivasaraghavan R[1], Seshadri S[2]*, Gnanasambandan T[2], Srinivasan G[4]

[1]*Department of Physics, SCSVMV University, Enathur, Kanchipuram 631561, India*
[2]*Department of Physics, Dr. Ambedkar Govt. Arts college, Vyasarpadi, Chennai-39, India*
[3]*Department of Physics, Pallavan College of Engineering, Kanchipuram-631502, India*
[4]*Department of Physics, Government Arts College, Nandanam, Chennai-35, India*

ABSTRACT

The fundamental modes complete vibration analysis and electronic properties of phenyl substituted compound N-((1-(phenylsulfonyl)-3-(phenylthio)-1H-indol-2-yl)methyl)acetamide have been investigated using the experimental spectroscopic techniques and quantum chemical studies. Density Functional Theory (DFT) method, using B3LYP functional, with 6-31G (d, p) and 6-311++G (d, p) basis sets, have been performed for assigning vibrational frequencies of the title compound, which in turn helps to derive useful information about the structure of the chosen compound. The experimentally obtained FTIR and FT Raman spectrum supports the results of theoretically observed ones. Detailed interpretations of the experimental spectra of the molecule along with the theoretical ones are reported based on Potential Energy Distribution (PED). Charge density distribution and site of chemical reactivity of the molecule have been analysed by mapping electron density is surface with Molecular Electrostatic Potential (MEP). The values of Mulliken atomic charges, Highest Occupied Molecular Orbitals-Lowest Lying Unoccupied Molecular Orbitals (HOMO-LUMO) energy gap are calculated. The intramolecular contacts are interpreted using Natural Bond Orbital (NBO) analysis to ascertain the charge distribution. The thermodynamic properties at different temperatures were calculated revealing the correlations between standard heat capacities, entropy and enthalpy changes with temperatures.

Keywords: N1P3P1HI2MA, Potential energy distribution, Natural bond orbital, NLMO, Molecular electrostatic potential

INTRODUCTION

Indole and its derivative compounds have been found to exhibit antibacterial, antifungal [1] and antitumor activities [2]. Some of the indole alkaloids extracted from plants possess interesting cytotoxic, antitumor or antiparasitic properties [3,4]. Pyrido[1,2-*a*] indole derivatives have been identified as potent inhibitors of human immunodeficiency virus type 1 [5] and 5-chloro-3-(phenylsulfonyl) indole-2-carboxamide is reported to be a highly potent non-nucleoside inhibitor of HIV-1 reverse transcriptase [6]. The interaction of phenyl sulfonyl indole with calf thymus DNA has also been studied by spectroscopic methods [7]. The molecular conformation in the solid state, X-ray studies of the title compound have been carried out by Thenmozhi et al. [8]. With this available literature background, a detailed information on experimental and theoretical investigation on the vibrational spectroscopic investigation and electron transitions of the compound have been carried out with Density Functional Theory (DFT) method using Gaussian 03W software [9] program. DFT method has been favorite due to its great accuracy in reproducing the experimental values of molecular geometry, vibrational frequencies, atomic charges, thermo dynamical properties etc., [10,11]. Among DFT calculation, Becke's three parameter hybrids functional combined with the Lee-Yang-Parr correlation functional (B3LYP) is the best predicting results for molecular geometry and vibrational wave numbers for moderately larger molecule [12,13]. Besides vibrational analysis, the other molecular parameters and electronic moment were studied in order to understand the overall activity of the molecule. The optimized geometry helps to calculate, energy gap, dipole moment, polarizability as well as first static hyperpolarizability components in order to understand the activity of the molecule. The theoretical quantum chemical calculations have also been performed to analyse Natural Bond Orbital (NBO) analysis, thermodynamic properties and Mulliken population analysis. The theoretically computed and experimental results were comparable with each other.

EXPERIMENTAL DETAILS

The compound under investigation N-((1-(phenylsulfonyl)-3-(phenylthio)-1H-indol-2-yl)methyl)acetamide was a synthesized one reported in literature [8] and used as such for recording Fourier Transform Infrared Spectroscopy (FTIR) and FT Raman spectra without further purification.

For FTIR spectral measurement, the sample was prepared in KBr pellet and the spectrum was collected at room temperature in the range of 4000-400 cm^{-1} with 4 cm^{-1} of resolution in evacuation mode using Bruker IFS 66V spectrophotometer. The FT-Raman spectrum is recorded in the same instrument with FRA 106 Raman module equipped with Nd: YAG laser source for excitation operating in stokes region at 1.064 nm line width. The laser spot was 200 μm in diameter and the power was kept at 30 mW to prevent and degradation. The spectrum is recorded in the 3500-100 cm^{-1}. The reported wave numbers of all sharp bands are expected to be accurate within ± 1 cm^{-1}.

Computational details

In our present work, the optimization of ground state molecular geometry and vibrational frequency calculations of N-((1-(phenylsulfonyl)-3-(phenylthio)-1H-indol-2-yl)methyl)acetamide [N1P3P1HI2MA], are performed using the Gaussian 03W program [13] with the B3LYP level of theory, supplemented with the standard 6-31 G (d,p) and 6-311++G (d,p) basis sets. The DFT method [14] has been employed using Becke's three parameter hybrid exchange function [15] with Lee-Yang-Parr correlation function [16,17] in order to optimize the structure in gas phase and to calculate the electronic structural properties of the molecule. The optimized structure of N-((1-(phenylsulfonyl)-3-(phenylthio)-1H-indol-2-yl) methyl) acetamide is shown in Figure 1. The molecular parameters of the optimized structure are shown in Table 1.

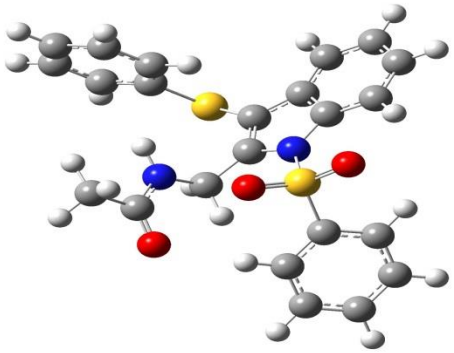

Figure 1: Optimized structure of N-((1-(phenylsulfonyl)-3-(phenylthio)-1H-indol-2-yl) methyl) acetamide

Table 1: Molecular parameters of N1P3P1HI2MA

Molecular parameters	Expt.	B3LYP/6-31G (d,p)	B3LYP/6-311++G (d,p)
H(50)-C(29)	1.08	1.12	1.09
H(49)-C(29)	1.07	1.12	1.09
H(48)-C(29)	1.07	1.12	1.23
H(47)-N(27)	1.00	0.99	1.36
H(46)-C(26)	1.07	1.13	1.09
H(45)-C(26)	1.07	1.13	1.10
H(44)-C(25)	1.07	1.10	1.08
H(43)-C(24)	1.08	1.10	1.09
H(42)-C(23)	1.07	1.10	1.09
H(41)-C(22)	1.06	1.10	1.09
H(40)-C(21)	1.07	1.10	1.09
H(39)-C(16)	1.08	1.10	1.09
H(38)-C(15)	1.07	1.10	1.09
H(36)-C(12)	1.07	1.10	1.09
H(35)-C(11)	1.06	1.10	1.09
H(34)-C(8)	1.07	1.10	1.08
H(33)-C(7)	1.07	1.10	1.09
H(32)-C(6)	1.07	1.10	1.09
O(30)-C(28)	1.26	1.24	1.23
C(29)-C(28)	1.50	1.51	1.52
C(28)-N(27)	1.34	1.39	1.36
N(27)-C(26)	1.48	1.44	1.46
C(26)-C(2)	1.53	1.52	1.50
C(25)-C(20)	1.37	1.40	1.40
C(25)-C(24)	1.37	1.39	1.39
C(24)-C(23)	1.36	1.40	1.40
C(23)-C(22)	1.36	1.40	1.40
C(22)-C(21)	1.36	1.39	1.40
C(21)-C(20)	1.35	1.40	1.40
C(20)-S(17)	1.81	1.72	1.79
O(19)-S(17)	1.46	1.43	1.46
O(18)-S(17)	1.47	1.45	1.46
S(17)-N(1)	1.55	1.52	1.56
C(16)-C(11)	1.42	1.39	1.40
C(16)-C(15)	1.38	1.40	1.40
C(15)-C(14)	1.40	1.39	1.39
C(14)-C(13)	1.40	1.40	1.40
C(13)-S(10)	1.80	1.70	1.80
C(13)-C(12)	1.39	1.40	1.40
C(12)-C(11)	1.42	1.39	1.40

S(10)-C(3)	1.79	1.76	1.77
C(9)-N(1)	1.31	1.31	1.32
C(9)-C(4)	1.39	1.43	1.42
C(9)-C(8)	1.42	1.44	1.40
C(8)-C(7)	1.42	1.36	1.39
C(7)-C(6)	1.40	1.42	1.41
C(6)-C(5)	1.38	1.37	1.39
C(5)-C(4)	1.42	1.42	1.40
C(4)-C(3)	1.36	1.41	1.41
C(3)-C(2)	1.36	1.34	1.37
C(28)-C(29)-H(48)	109.8	110.4	110.4
C(28)-C(29)-H(49)	109.3	110.1	109.9
C(28)-C(29)-H(50)	109.8	108.5	109.3
H(48)-C(29)-H(49)	109.7	109.2	109.6
H(48)-C(29)-H(50)	109.5	109.0	109.6
H(49)-C(29)-H(50)	108.8	108.9	108.9
N(27)-C(28)-C(29)	121.6	121.9	121.3
N(27)-C(28)-O(30)	118.6	119.6	119.4
C(29)-C(28)-O(30)	119.7	120.5	119.9
C(26)-N(27)-C(28)	119.2	120.1	120.1
C(26)-N(27)-H(47)	119.9	118.4	119.2
C(28)-N(27)-H(47)	121.0	119.9	120.1
C(2)-C(26)-N(27)	110.3	112.7	111.2
C(2)-C(26)-H(45)	109.7	110.7	110.1
C(2)-C(26)-H(46)	109.0	110.4	110.6
N(27)-C(26)-H(45)	108.9	109.2	109.1
N(27)-C(26)-H(46)	109.6	109.3	109.4
H(45)-C(26)-H(46)	109.3	109.3	109.3
H(44)-C(25)-C(20)	120.5	119.1	120.4
H(44)-C(25)-C(24)	119.2	120.0	120.2
C(20)-C(25)-C(24)	120.3	120.8	120.6
H(43)-C(24)-C(25)	120.7	120.1	120.7
H(43)-C(24)-C(23)	119.6	120.1	120.2
C(25)-C(24)-C(23)	119.7	119.8	120.1
H(42)-C(23)-C(24)	120.2	120.0	119.7
H(42)-C(23)-C(22)	120.1	120.0	119.9
C(24)-C(23)-C(22)	119.8	119.9	120.4
H(41)-C(22)-C(23)	119.8	120.1	120.3
H(41)-C(22)-C(21)	119.5	120.1	119.3
C(23)-C(22)-C(21)	120.7	119.8	120.4
H(40)-C(21)-C(22)	119.8	120.0	120.1
H(40)-C(21)-C(20)	119.8	119.2	119.7
C(22)-C(21)-C(20)	120.3	120.9	120.8
S(17)-C(20)-C(25)	121.6	120.3	121.6
S(17)-C(20)-C(21)	119.3	120.1	119.2
C(25)-C(20)-C(21)	119.1	118.7	120.2
O(18)-S(17)-O(19)	121.2	121.6	121.5
O(18)-S(17)-N(1)	109.2	110.1	110.2
O(18)-S(17)-C(20)	108.7	108.6	108.5
O(19)-S(17)-N(1)	107.6	108.7	108.1
O(19)-S(17)-C(20)	107.9	108.5	108.2
N(1)-S(17)-C(20)	113.2	114.8	113.9
H(39)-C(16)-C(11)	121.0	120.1	120.3
H(39)-C(16)-C(15)	120.1	120.0	120.3
C(11)-C(16)-C(15)	119.9	119.9	119.4
H(38)-C(15)-C(16)	120.7	120.1	120.1
H(38)-C(15)-C(14)	119.8	119.8	119.9
C(16)-C(15)-C(14)	120.5	120.1	120.5
C(15)-C(14)-C(13)	119.8	120.1	120.1
S(10)-C(13)-C(14)	116.2	115.4	116.3
S(10)-C(13)-C(12)	123.2	123.8	123.5
C(14)-C(13)-C(12)	120.6	119.7	119.6
H(36)-C(12)-C(13)	120.8	119.9	120.1
H(36)-C(12)-C(11)	120.5	120.0	120.1
C(13)-C(12)-C(11)	119.7	120.1	119.8
H(35)-C(11)-C(16)	119.4	120.2	120.1
H(35)-C(11)-C(12)	119.4	119.6	119.2
C(16)-C(11)-C(12)	121.2	120.1	120.6
C(3)-S(10)-C(13)	118.1	115.6	117.7
N(1)-C(9)-C(4)	123.5	123.8	123.9
N(1)-C(9)-C(8)	123.3	123.3	123.3
C(4)-C(9)-C(8)	117.1	115.9	117.1
H(34)-C(8)-C(9)	118.6	117.8	119.5
H(34)-C(8)-C(7)	120.8	120.4	120.9
C(9)-C(8)-C(7)	120.6	120.8	120.5

H(33)-C(7)-C(8)	120.5	120.4	120.7
H(33)-C(7)-C(6)	119.4	118.5	119.4
C(8)-C(7)-C(6)	121.1	121.1	121.9
H(32)-C(6)-C(7)	119.8	119.3	119.6
H(32)-C(6)-C(5)	118.0	119.2	119.2
C(7)-C(6)-C(5)	120.2	119.6	120.5
C(6)-C(5)-C(4)	120.6	120.6	120.7
C(3)-C(4)-C(9)	120.9	119.6	120.3
C(3)-C(4)-C(5)	120.8	120.4	120.4
C(9)-C(4)-C(5)	120.3	120.0	120.3
C(2)-C(3)-C(4)	121.0	120.8	120.6
C(2)-C(3)-S(10)	115.4	113.9	115.8
C(4)-C(3)-S(10)	123.6	124.2	123.8
C(3)-C(2)-C(26)	119.9	120.0	119.8
C(9)-N(1)-S(17)	123.0	123.7	123.5

At the optimized structural orientation, the vibrational wave numbers are also calculated. These wavenumbers scaled down by proper scaling factor in order to equate the values with the experimental ones [18,19]. The assignments along with Price Elasticity of Demand (PED) calculations have been carried out by combining the results of the Gauss view 5 programs [20], symmetry considerations and using VEDA 4 program [21]. The Raman intensities obtained from the results of Gaussian 03W are converted into the Raman activities (Si), using the following relationship [22,23].

$$Ii=[f(\nu_0-\nu_i)^4 Si]/[\nu_i\{1-\exp(-hc\,\nu_i/kT)\}]$$

Where ν_0-exciting wave number in cm^{-1}, ν_i-the vibrational wave number of the normal mode, h, c and k universal constants and f is a suitably chosen common normalization factor for all peak intensities. A Raman spectrum has been calculated according to the spectral database reported by the Sigma Aldrich chemical website [24]. The calculated FTIR and Raman spectra have been plotted using the pure Lorentzian band shape with a band width of 10 cm^{-1} FWHM along with the experimentally observed one and are shown in Figures 2 and 3. The Natural Bonding Orbitals (NBO) calculations [25] are performed using NBO 3.1 program, which is a measure of the intermolecular delocalization or hyper conjugation. Density functional theory DFT-G03W has also been used to calculate the dipole moment μ, mean polarizability <α> and first static hyperpolarizability β. Following Buckingham's definitions [26], the total dipole moment and the mean polarizability is defined as:

$$\mu=(\mu_x^2+\mu_y^2+\mu_z^2)^{1/2}$$

$$<\alpha>=1/3\,[\,\alpha_{xx}+\alpha_{yy}+\alpha_{zz}]$$

The total intrinsic hyperpolarizability β_{TOTAL} [27] is defined as: $\beta_{TOTAL}=[\beta_x^2+\beta_y^2+\beta_z^2]^{1/2}$. Where, $\beta_x=\beta_{xxx}+\beta_{xyy}+\beta_{xzz}$, $\beta_y=\beta_{yyy}+\beta_{yzz}+\beta_{yxx}$, $\beta_z=\beta_{zzz}+\beta_{zxx}+\beta_{zyy}$.

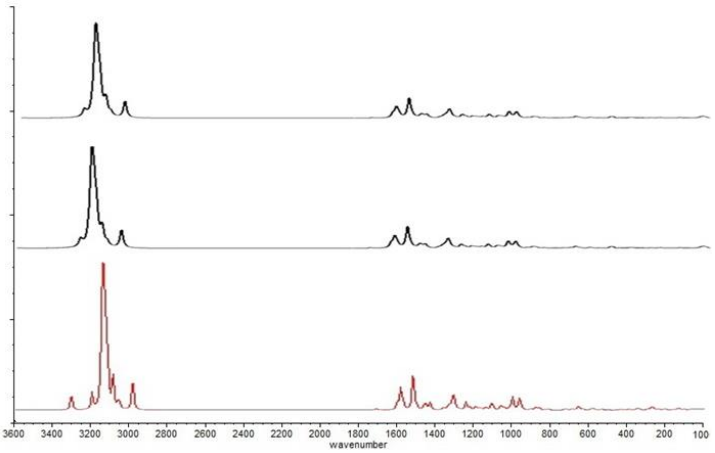

Figure 2: Experimental and Theoretical IR spectra of N-((1-(phenylsulfonyl)-3-(phenylthio)-1H-indol-2-yl)methyl)acetamide

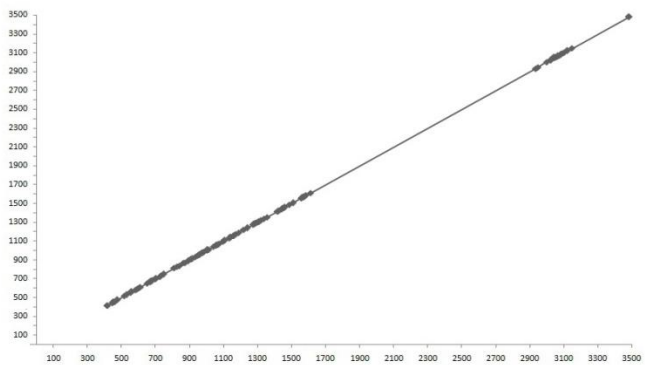

Figure 3: Experimental and Theoretical Raman spectra of N-((1-(phenylsulfonyl)-3-(phenylthio)-1H-indol-2-yl)methyl)acetamide

Vibrational assignments

The optimized structure of N1P3P1HI2MA has 50 elements and it should possess 144 normal modes of vibration with C_1 point group symmetry. The functional group and fingerprint regions of N1P3P1HI2MA are confirmed by experimentally recorded the FT-IR spectrum in the range 4000-400 cm^{-1} and FT Raman spectrum in the range 3500-100 cm^{-1}. The fundamental harmonic vibrations were studied using B3LYP/6-31 G (d,p) and B3LYP/6-311++G (d,p) basis sets along with PED values and are summarized in Table 2 along with experimental data. It is usual that the calculated vibrational wave numbers are higher than experimental values for the majority of the normal modes. The calculated wave numbers are scaled down using single scaling factor 0.961 to discard of any harmonicity present in real system [28]. In order to justify the theoretical wavenumbers, a detailed analysis of experimental and theoretically calculated wavenumbers are carried out. The correlation graph is shown in Figures 3 and 4. The value of correlation coefficient found to be r=0.999, showing good agreement with the calculated wave numbers with experimental. Most of modes are not pure but contains significant contributions from other modes also. The Potential Energy Distribution (PED) and modes obtained from Gauss-View program helps in the assignment of calculated harmonic frequencies and peaks of the experimental FTIR and FT Raman spectrum.

Table 2: Theoretical and experimental vibrational analysis table of N1P3P1HI2MA

FTIR ν (cm^{-1})	FT Raman	B3LYP/6-31G (d, p)			B3LYP/6-311++G (d, p)			Assignment with PED (%)
		ν (cm^{-1})	IR inten	Raman int	ν (cm^{-1})	IR inten	Raman int	
		16	0.703	83.575	17	0.190	6.217	Assignment with PED (%)
		19	1.195	66.945	20	0.491	3.421	
		29	1.217	99.317	28	0.720	4.403	τ ring (16)
		33	0.477	56.495	33	0.328	10.665	ring sci (21)
		42	3.820	88.022	42	1.149	5.958	τ ring 2 (24)
		46	0.478	78.248	45	1.174	2.832	τ ring 3 (23)
		49	1.383	80.674	49	0.798	5.332	τ CS (19)
		57	1.283	65.217	59	0.917	3.326	Ring bre. (11)
		79	2.640	24.708	80	4.674	2.151	βring (17)
		88	0.758	52.842	90	9.234	2.182	τ ring 2 (29)
		98	1.174	7.389	98	0.741	0.398	Ring bre. (16)
	120	121	4.253	1.779	123	0.346	0.992	τ CS (16)
	149	147	0.972	0.976	145	0.513	4.807	τ CS (23)
	156	154	0.201	2.999	155	0.182	4.219	τ CH_3 (18)
	165	163	4.964	1.704	163	4.227	1.137	β SO_2 (17)
	175	174	7.688	3.195	174	2.120	1.136	τ ring 1 (26)
	187	186	3.775	1.874	186	4.032	2.472	γ CS (18)
		188	0.784	4.019	187	3.907	1.217	τ ring 3 (15)
	205	205	0.742	3.122	205	1.155	1.224	τ ring (24)
	221	220	1.940	32.833	221	3.435	2.735	τ CN (27)
	246	245	3.630	29.146	244	1.150	6.651	τ SO_2 (29)
	261	260	11.524	2.105	262	0.492	5.215	β ring 2 (19)
	290	289	7.287	5.695	290	1.122	1.748	τ CH_2 (23)
	300	297	26.404	11.360	297	2.229	4.482	β ring 3 (22)
	307	305	5.519	12.969	304	2.236	1.504	CH_2 sci. (31)
	326	324	29.272	4.008	326	1.696	3.813	τ ring (20)
	345	347	90.302	1.994	348	5.166	1.692	τ NH (24)
	372	375	5.450	5.228	374	0.596	0.395	CH_2 sci. (26)
		386	0.295	1.245	385	2.022	0.582	τ CN (18)+α CCC (19)
	394	397	0.661	1.146	397	0.030	0.340	τ NH (21)
412		415	2.306	1.816	415	5.587	0.795	τ ring 3 (24)
	419	419	53.538	1.290	418	2.117	1.407	τ ring 2 (13)
445		443	23.294	39.439	442	6.425	0.930	τ CN (22)
	447	447	26.688	87.799	445	48.770	1.703	τ ring 3 (25)
452		451	23.149	0.328	451	12.512	2.765	β Ring (21)
	459	458	3.484	3.133	457	3.657	2.099	γ CN (68)
476	476	475	21.371	1.693	475	22.199	2.265	γ CN (13)
514	516	516	16.268	13.302	516	21.423	3.204	γ ring 4 (27)
530	530	529	50.967	2.163	529	62.335	0.888	δ NS (63)+α CCC (19)
553	552	552	57.027	2.868	550	98.723	6.230	δ ring 4 (21)
560	562	561	57.527	4.195	561	20.627	1.239	τ NC (11)+β CCO (25)
581	580	581	76.356	2.664	580	5.449	1.184	β ring (22)+α CCC (19)
590		589	45.401	1.504	588	18.340	3.001	γ CH (17)+γ CN (13)
	596	597	14.339	0.488	597	0.546	6.044	ν CS (65)
603	603	602	94.891	6.436	602	0.635	3.827	γ CO (35)+τ NC (18)
610		609	15.694	3.537	609	0.266	2.168	γ NH (34)
649	649	650	2.038	4.830	649	12.760	7.325	ν CBr (47)
667		666	0.250	0.685	665	2.482	5.043	γ CC (21)
	670	670	48.336	2.806	669	44.399	2.149	γ CN (32)
672	673	673	52.526	0.816	672	26.905	14.837	β CCN (21)
678		677	99.190	0.858	675	12.985	1.308	β NCH (29)
695	696	695	99.893	0.566	694	61.652	4.030	γ CC (18)
703	702	701	10.846	2.191	700	47.747	3.001	γ CH (23)

723	721	722	8.104	0.754	722	42.407	2.063	ν CS (66)
730		731	28.128	4.843	731	27.908	2.642	β ring (13)
	733	734	71.262	6.769	733	22.882	3.407	γ CH (48)+γ CN (9)
746	745	747	56.268	8.479	746	14.682	0.614	γ CH (54)+γ NCO (19)
810	813	813	84.930	3.709	816	0.335	3.824	ν CC(23)
829	829	827	81.448	1.709	827	2.311	3.408	γ CH (79)
841		840	53.987	5.022	839	0.070	2.807	γ CN (16)+β CNH (14)
865	865	866	7.958	5.473	866	26.430	10.998	γ CC (31)+τ ring (12)
872		871	1.628	9.702	872	3.049	2.410	γ SO (49)
890	890	889	44.463	1.404	885	16.280	15.612	γ SO(45)
908		908	44.059	5.367	909	19.862	5.523	ν CN (23)
	910	910	1.116	6.637	910	9.407	0.769	ν CC (65)
913		912	0.106	4.825	911	7.098	0.824	γ CN (24)
933	934	934	5.753	5.637	931	0.333	0.343	γ CH (42)
946	945	945	0.174	40.682	945	0.056	0.248	γ CC (11)
	952	952	9.697	33.728	952	3.766	1.376	γ CH (29)
955		954	22.228	12.928	954	0.123	0.399	ν CC (67)
957	957	957	6.167	1.019	957	7.777	6.425	ν CN (35)
	963	962	0.069	8.452	963	1.568	18.728	γ CO (14)
	968	968	7.673	100.379	967	4.333	43.786	β CCH (9)
975	975	975	43.193	63.427	976	7.534	6.542	γ CH (37)+β CCC (29)
985	985	983	4.686	85.097	982	18.611	3.745	νCC (69)
1003	1003	1002	95.070	100.131	1002	1.270	26.725	τring (11)
1005	1005	1005	22.519	100.571	1004	13.187	25.354	β CCH (41)
1008		1008	41.874	26.404	1007	17.536	22.791	νCC (71)
1013	1013	1012	15.681	4.393	1013	5.549	0.904	β NCH (16)+β ring (21)
1039	1039	1038	23.342	0.863	1039	14.008	10.403	δ SO (30)
1053	1054	1053	1.751	55.288	1050	60.426	9.480	β CCH (16)+β ring(11)
1059	1059	1058	48.241	100.489	1057	43.175	8.879	β NCH (27)+β CCH (17)
1062		1061	1.719	2.558	1061	17.526	10.768	ν CC(53)
1067	1067	1066	2.457	18.817	1066	7.274	1.402	ν CN (61)
1072		1071	31.671	10.575	1071	43.475	0.876	β CCH (26)
1096	1096	1095	43.508	2.409	1096	2.556	5.841	ν CC (52)
1107	1107	1106	0.045	15.151	1105	88.382	40.485	β CCH (22)
1132	1132	1131	9.958	3.387	1131	16.465	6.342	β CCH (23)
1138	1138	1137	1.051	11.265	1136	0.316	6.047	ν CC (65)
1143	1142	1142	5.694	6.330	1141	0.258	5.914	ν_s SO (73)
1156	1156	1157	4.746	13.781	1157	2.746	3.444	δ CH (57)
1161	1160	1160	5.819	3.352	1160	7.363	5.509	β CCH (23)+β CCO (18)
1172	1171	1171	10.796	2.324	1172	76.122	11.442	β CCH (41)+β CCC (14)
1189	1190	1189	33.467	3.492	1188	53.571	18.450	β NCH (38)
1218	1217	1219	16.008	0.982	1219	96.108	15.868	ν CN (51)
1239	1244	1240	3.731	8.412	1239	63.616	38.744	ν CC (83)
1272	1274	1272	1.606	28.688	1270	2.226	3.113	ν_a SO (69)
1279		1279	13.608	5.515	1277	17.151	4.061	β CCH (83)
1285	1285	1286	31.358	28.040	1287	3.294	1.567	ν CN (41)
1298	1299	1298	6.091	21.586	1297	63.219	29.547	ν CN (45)
1303		1302	5.437	54.482	1300	17.438	10.411	β CCC (21)
1305	1305	1306	12.572	10.439	1305	34.978	66.705	ν CN (83)
1312	1313	1313	99.860	36.377	1312	48.866	9.546	ν CC (77)+β CCH (41)
1321	1323	1322	10.282	55.411	1322	17.077	18.910	ν CN (66)+β HCH (49)
1336	1336	1335	90.871	62.173	1331	3.067	16.146	ν CC (62)+β CCH (13)
1357	1356	1354	26.955	10.114	1349	23.005	10.114	νCC (52)
1415	1413	1413	43.481	52.282	1416	34.799	27.683	νCN (57)+ β CCC (28)
1418		1417	78.830	12.543	1417	10.173	4.267	ν CN (61)
1422		1420	27.309	8.144	1420	26.952	8.618	ρ CH (22)
1426	1426	1425	30.641	1.775	1424	18.451	1.372	α CH_3 (16)+ν CC (83)
1439	1438	1438	31.626	7.886	1437	14.874	13.721	β CCH (47)
1445	1445	1443	19.457	5.201	1442	20.411	25.287	β CCH (59)+ν CC (73)
1453		1452	90.119	2.443	1451	3.444	9.911	β CCH (18)+ν CC(76)
1455		1454	75.537	2.805	1454	43.410	0.513	β HCH (29)+β NCH(13)
1458	1459	1457	80.171	6.124	1456	6.949	1.460	β NH_2 (32)+ν CC s (78)
1486	1486	1486	90.049	100.029	1486	99.978	18.999	β NH_2 (41)
1507	1503	1505	0.300	27.367	1505	34.133	99.741	ν CC s (94)
1556	1556	1557	1.152	36.190	1555	4.695	30.653	ν CC s (95)
1561	1561	1560	18.216	7.829	1559	1.683	11.089	ν CC s (91)
1569	1569	1568	102.650	3.049	1567	0.777	39.479	ν CC (95)
1572	1572	1571	167.098	16.684	1570	0.816	21.844	ν CC as (92)
1578	1578	1578	100.073	3.668	1579	44.258	50.282	ν CC as (95)
1583	1583	1584	97.431	0.309	1586	7.678	43.411	ν CC as (91)
1609	1609	1608	93.631	0.147	1610	100.438	7.012	ν C=C (93)+β NH2 (37)

2936	2933	2931	97.075	0.880	2926	8.243	92.436	ν C=N (91)
2949	2948	2945	76.326	1.876	2947	7.509	71.010	ν C=O (87)
2999	2998	3000	17.475	8.872	2996	11.168	41.605	ν CH (99)
3021	3018	3019	9.225	23.069	3020	10.652	90.689	ν CH (99)
3024		3022	38.606	18.865	3023	2.553	98.537	ν CH (99)
3046	3046	3045	42.962	5.770	3043	2.100	19.129	ν CH (99)
	3049	3049	13.518	1.323	3048	3.734	73.432	ν CH_2 s (99)
3052		3051	38.119	8.787	3051	2.239	85.973	ν CH s (99)
3055	3055	3054	24.908	25.956	3053	3.896	53.554	ν CH (99)
3059		3059	20.734	26.700	3058	15.027	88.599	ν CH s (99)
3062	3062	3061	23.396	100.815	3061	16.289	90.924	ν CH3 s (99)
3065		3064	41.051	22.431	3064	40.160	89.987	ν CH (99)
3072		3071	10.291	6.214	3070	0.502	61.009	ν CH (99)
3077	3077	3076	10.157	49.424	3075	16.871	92.953	ν CH s (98)
3082	3083	3081	86.419	15.877	3081	19.545	96.732	ν CH (98)
3092		3090	54.680	6.356	3089	11.270	100.010	ν CH as (98)
3100	3100	3099	78.978	9.743	3098	19.848	94.810	ν CH2 as (99)
3121	3122	3120	38.006	33.735	3121	6.967	88.637	ν CH (99)
3148	3146	3145	65.125	1.351	3145	2.855	77.206	ν CH_3 as (98)
3483	3480	3479	87.467	6.559	3478	64.650	90.041	ν CH as (99)

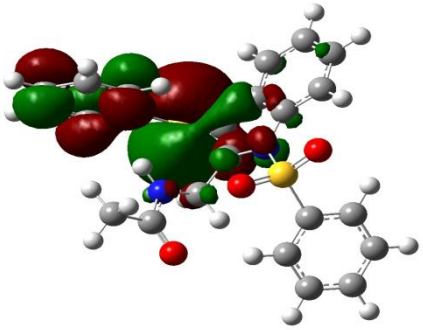

Figure 4: Correlation graph between experimental and calculated wave numbers of N-((1-(phenylsulfonyl)-3-(phenylthio)-1H-indol-2-yl)methyl)acetamide

C-H vibrations

In aromatic compounds, the position of C-H stretching vibrations are the most stable in the spectrum and are observed around 3200-2950 cm^{-1} [29-32]. The compound N1P3P1HI2MA exhibit C-H symmetric stretching vibrations at 3046 and 3065 cm^{-1} and the asymmetric stretching vibrations occur in the region at 3121 and 3148 cm^{-1} respectively. The other C-H vibrational bands in the range are assigned to the symmetric and asymmetric modes respectively. All the bands are in coincident with the theoretically calculated wave numbers using B3LYP/6-31G (d, p) and B3LYP/6-311++G (d, p) basis sets. The C-H in-plane and out-of-plane bending vibrations generally lie in the range 1300-1000 cm^{-1} and 1000-800 cm^{-1} [33,34], respectively. In our title compound, the calculated wave numbers at 1303, 1239 cm^{-1} are assigned as C-H in plane bending vibrations and the bands observed at 963, 746 cm^{-1} may be due to C-H out of plane bending vibrations. According to the literature [33,34], the in plane and out-of-plane bending vibrations observed are within their characteristic regions and the theoretically values coincide with the experimentally observed ones.

N-H vibrations

In dilute solutions of non-polar solvents, primary amines show moderate intense N-H stretching vibrations in the range between 3550-3400 cm^{-1} corresponding to the symmetrical and antisymmetrical N-H stretching vibrations. In the spectra of solid samples, these bands are observed near 3350 and 3200 cm^{-1} because of hydrogen bonding. In the IR spectra of secondary amines, which exist mainly due to the trans conformation of the free N-H stretching vibration occurred in dilute solutions, occur nearly 3500-3400 cm^{-1}. In more concentrated samples, the free NH band is replaced by multiple bands in the region 3400-3100 cm^{-1} [35]. Puviarasan et al. [36] have observed the IR bands at 3283 and 3329 cm^{-1} in 3-aminophthalhydrazine as N-H stretching vibrations. The bands at 3420 and 3456 cm^{-1} have been assigned to NH_2 symmetric and asymmetric stretching vibrations respectively for the same compound. Considering the above references, in the present investigation, the band observed at 3483 cm^{-1} in the FTIR spectrum of N1P3P1HI2MA is assigned to N-H stretching mode of vibration.

The N-H bending vibration of primary amines is observed in the region 1650-1580 cm^{-1} [37]. The band observed with medium strong intensity at 1578 cm^{-1} in the FTIR spectrum is expected to be due to amine deformation. Secondary aliphatic amines C-N-H deformation in the range 850-750 cm^{-1}. According to this literature, the band at 810 cm^{-1} is assigned to C-N-H deformation.

C-C ring stretching

Benzene has two doubly degenerate modes and two non-degenerate modes of vibration due to stretching [38,39] of C-C bonds. The ring C-C stretching vibrations occur in the region 1625 cm^{-1}-1430 cm^{-1}. In the present work the bands observed at 1426 cm^{-1} and 1556 cm^{-1} in the FTIR spectrum and the bands at 1426 cm^{-1} and 1556 cm^{-1} in FT Raman spectrum are assigned to ring C-C symmetric and asymmetric stretching vibrations respectively. The calculated values of C–C–C in–plane bending modes are presented at 553, 476 and 345 cm^{-1}. Some of these vibrations appear with mixed modes. The C–C–C out–of–plane bending vibrations are assigned below 200 cm^{-1}. The CCO-deformation mode is observed at 530 cm^{-1} in infrared region and the same at 529 cm^{-1} is observed in theoretically computed values [40].

C-N vibrations

The identification of C-N and C=N vibrations is a difficult task, since the mixing of vibrations is possible in this region. Silverstein et al. [37] assigned the C-N stretching absorption in the range 1400-1250 cm^{-1} for aromatic amines. Similarly for C=N stretching mode in the range between 1450-1550 cm^{-1} [41]. In the present work, the bands observed at 1298, 1357 cm^{-1} in FT-IR spectrum are assigned to C-N stretching vibrations. The theoretically computed value of C-N stretching vibrations also falls in the same region with the predicted values of 1298 and 1354 cm^{-1} by B3LYP/6-31G (d, p) and B3LYP/6-311++G (d, p) methods. The C=N stretching vibration band occurs in the region 1583 cm^{-1} and the computationally calculated value matches with the experimentally observed.

C=O vibration

The band due to C=O stretching vibration is observed in the region 1700-1550 cm^{-1}. Because of its high intensity [42,43] and its occurrence in relatively interference free region, this band is reasonably easy to recognize. In the present work, the band observed at 1609 cm^{-1} in FTIR and in Raman spectrum is assigned to C=O stretching mode of vibration. In general all amides have one or more bands in the region 725-600 cm^{-1} which are more probably due to the bending motion of the N-C=O group [44]. The band observed at 609 cm^{-1} in FTIR spectra is assigned to N-C=O symmetric bending and the band at 730 cm^{-1} in FTIR and at 731 cm^{-1} in FT Raman spectra are assigned to N-C=O bending of N1P3P1HI2MA molecule.

Mulliken atomic charges

The Mulliken atomic charge for the present compound is calculated at the B3LYP/6-31G (d, p) and B3LYP/6-311++G (d, p) levels in gas phase and are presented in Figure 5. The Mulliken atomic charge directly relates the vibrational properties of any molecule and in turn affects its dipole moment, polarizability, electronic structure and more properties of molecular system [45,46]. The natural charge distribution of N1P3P1HI2MA exhibits more negative towards oxygen atoms (-0.531 and -0.530) as compared to nitrogen atoms (-0.477 and -0.445). The charge of the O atoms of the S=O group are -0.531 and -0.515, while the charge across S atom is calculated as 1.282 in that group. On the other hand, the charges of few C and N atoms are negative; however these negative charges are lower than that observed for O and N atoms. In N1P3P1HI2MA, C_2, C_4, C_8, C_9, C_{11}, C_{14} and C_{15} are positively charged atoms, while the remaining C atoms are negatively charged. Such a type of charge distribution generates the total dipole moment of 1.9831 Debye for N1P3P1HI2MA compound. The total atomic charges of N1P3P1HI2MA obtained by using B3LYP/6-31G (d, p) and B3LYP/6-311++G (d, p) methods are listed in Table 3.

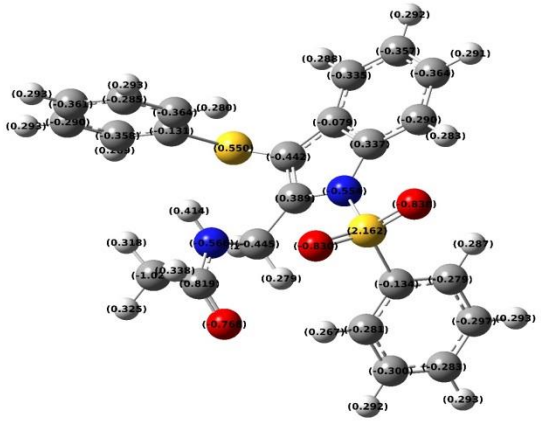

Figure 5: Mulliken atomic charge distribution of N-((1-(phenylsulfonyl)-3-(phenylthio)-1H-indol-2-yl) methyl) acetamide

Table 3: Mulliken atomic charges of N1P3P1HI2MA

Atom	B3LYP/6-31G (d, p)	B3LYP/6-311++G (d, p)	Atom	B3LYP/6-31G (d, p)	B3LYP/6-311++G (d, p)
C	0.314796	0.054882	N	-0.51259	-0.394621
C	-0.267041	-0.076364	C	0.59913	0.298633
C	0.082971	-0.220314	C	-0.39658	-0.241318
C	-0.135999	-0.053762	O	-0.53039	-0.553151
C	-0.090939	-0.209474	H	0.104184	0.128485
C	-0.108909	-0.043303	H	0.085984	0.133848
C	-0.087067	-0.242246	H	0.088473	0.130215
C	0.287603	0.374519	H	0.133688	0.140084
S	0.147983	0.369797	H	0.09577	0.146249
C	-0.084114	-0.120281	H	0.111873	0.1597
C	-0.117432	-0.100653	H	0.100607	0.142328
C	-0.106177	-0.294118	H	0.093496	0.141151
C	-0.097485	-0.103381	H	0.090824	0.140958
C	-0.076573	-0.126094	H	0.183257	0.142596
C	-0.090739	-0.109902	H	0.113473	0.131313
S	1.282459	1.518219	H	0.103943	0.128514
O	-0.531504	-0.564622	H	0.105528	0.133097
O	-0.515479	-0.583447	H	0.128753	0.150365
C	-0.195367	-0.387985	H	0.144841	0.150011
C	-0.086643	-0.02298	H	0.148423	0.285406
C	-0.09446	-0.160999	H	0.268046	0.223558
C	-0.071362	-0.083031	H	0.105408	0.097364
C	-0.088509	-0.158901	H	0.141003	0.105955
C	-0.090355	-0.000552	H	0.155051	0.124479

Electric moments

Most of the organic molecules that are having conjugated π-electron systems are characterized hyperpolarisibilities has been analysed by means of vibrational spectroscopy [47,48]. The main focus of the molecule demands investigation about its molecular parameters that contributes the hyperpolarizability, in turns help to study the vibrational modes and for our compound B3LYP/6-31G (d, p) and B3LYP/6-311++G (d, p) methods were used for the prediction of first order hyperpolarizability (β). The tensor components of the static first order hyperpolarizability (β) were analytically calculated by using the same method as mentioned above. The components of polarizability and the first order hyperpolarizability of the title compound are given in Table 4.

Table 4: The calculatedμ, α and β components of N1P3P1HI2MA

Parameters	B3LYP/6-31G (d, p)	B3LYP/6-311++G (d, p)	Parameters	B3LYP/6-31G (d, p)	B3LYP/6-311++G (d, p)
μ_{ξ}	-0.5669	0.2913	$\beta_{\xi\xi\xi}$	525.365	468.462
μ_{ψ}	-0.4642	0.4639	$\beta_{\xi\xi\psi}$	-113.284	-103.568
μ_{ζ}	1.8428	1.1965	$\beta_{\xi\psi\psi}$	127.467	93.121
μ	1.9831	2.8576	$\beta_{\psi\psi\psi}$	50.98	-73.871
$\alpha_{\xi\xi}$	340.124	314.578	$\beta_{\xi\xi\zeta}$	-87.861	76.119
$\alpha_{\xi\psi}$	-17.293	19.198	$\beta_{\xi\psi\zeta}$	70.865	29.085
$\alpha_{\psi\psi}$	326.674	223.401	$\beta_{\psi\psi\zeta}$	-81.231	56.614
$\alpha_{\xi\zeta}$	12.425	11.185	$\beta_{\xi\zeta\zeta}$	23.657	11.969
$\alpha_{\psi\zeta}$	10.159	-26.947	$\beta_{\psi\zeta\zeta}$	-21.493	19.483
$\alpha_{\zeta\zeta}$	223.834	197.751	$\beta_{\zeta\zeta\zeta}$	-16.765	-12.976
$\alpha_{\tau\sigma\tau}$	296.877	245.243	$\beta_{\tau\sigma\tau}(\varepsilon\sigma\upsilon)$	1.643×10^{-30}	1.735×10^{-30}
Δα	689.164	533.465			

FMO-global reactivity descriptors

The most important orbitals in molecule for reactivity are the two so called frontier orbitals Highest Occupied Molecular Orbitals (HOMOs) and Lowest-lying Unoccupied Molecular Orbitals (LUMOs) [49]. According to the theory, chemical reactivity, transition of electrons is due to interaction between HOMO and LUMO of reacting species [50]. The FMOs have an important role in the electric and optical properties, as well as in quantum chemistry, chemical reactions and UV-VIS spectra [49]. The HOMO shows that the charge density localized mainly on carbonyl and amine group whereas LUMO is localized on ring system. There is an energy gap between HOMO and LUMO. This energy gap in turn helps to determine the kinetic stability, chemical reactivity, optical polarizability and chemical hardness–softness of a molecule. The energy gap is large for hard molecules and small for soft molecules [51,52]. A molecule with low energy gap is more polarizable and is generally associated with the high chemical activity and low kinetic stability [50]. The distributions of the HOMO and LUMO were computed at the 6-31G (d, p) and 6-311++G (d, p) for the title molecule and are given in Table 5.

Table 5: Molecular properties of, N1P3P1HI2MA

Molecular properties	B3LYP		Molecular properties	B3LYP	
	6-31G (d, p)	6-311++G (d, p)		6-31G (d, p)	6-311++G (d, p)
E_{HOMO} (eV)	-5.8406	-8.0530	Chemical hardness (η)	2.2393	2.9304
E_{LUMO} (eV)	-1.3619	-2.1921	Softness (S)	0.4465	0.3413
$E_{HOMO-LUMO}$ gap (eV)	4.4787	5.8608	Chemical potential (μ)	-3.6013	-5.1225
Ionisation potential (I) eV	5.8406	8.0530	Electronegativity (χ)	3.6013	5.1225
Electron affinity(A) eV	1.3619	2.1921	Electrophilicity index (ω)	6.4847	13.1201

To understand the bonding feature of the title molecule, the plot of the frontier orbitals, HOMO and LUMO are shown in Figure 6. The calculations indicate that the title molecule has 114 occupied molecular orbitals. The value of the energy separation between the HOMO and LUMO are 4.4787 and 5.8608 eV for 6-31G (d, p) and 6-311++G (d, p) basis sets respectively. This large energy gap indicates that the title molecule is quite stable. Various qualitative chemical concepts like electronegativity (χ), chemical hardness (η), chemical softness (S), electrophilicity index (ω) and chemical potential (μ) have been calculated using the energies of the frontier orbital with the help of DFT method. The ionization potential (I) and electron affinity (A) can be expressed as with the help of E_{HOMO} and E_{LUMO} as I=-E_{HOMO} and A=-E_{LUMO}., according to the Koopman's theorem [53]. It is assumed that these relations are valid within the DFT frame. The electronegativity, hardness and chemical potential can be estimated with the formula:

$$\eta=\frac{I-A}{2} \qquad \mu=\frac{-(I+A)}{2} \qquad \chi=\frac{I+A}{2}$$

The softness (σ) is also given by σ=1/η [54]. The absolute electrophilicity index (ω) is defined as:

$$\omega=\frac{\mu^2}{2}$$

Considering the chemical hardness, if the result of HOMO-LUMO gap is high then it can be called as a hard molecule instead for smaller gaps it is called as soft molecule. These low values are more reactive in terms of the stability of the molecule. Using the above equations, the chemical potential, hardness and electrophilicity index have been calculated for N1P3P1HI2MA and their values are shown in Table 4. The calculated value of electrophilicity index describes the biological activity of N1P3P1HI2MA [55-57].

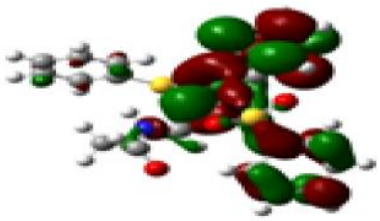

Figure 6: HOMO and LUMO diagram of N-((1-(phenylsulfonyl)-3-(phenylthio)-1H-indol-2-yl)methyl)acetamide

Molecular Electrostatic Potential (MEP)

The MEP is the force acting on a proton through the electrical charge cloud generated through the molecules, electrons and nuclei. Despite the fact that the molecular charge distribution remains unperturbed, the electrostatic potential of a molecule is still a good guide in assessing the molecules reactivity towards positively or negatively charged reactants. It is the graphic tool of total electron density surface mapped with the electrostatic potential, the sign of the electrostatic potential in a surface region is determined by the predominance of negative or positive charges contribution. It is related to the total charge distribution of the molecule proving the correlations between the molecular properties such as dipole moments, partial charges, chemical reactivity and electronegativity of molecules.

Accordingly, it is possible to identify regions that are more susceptible to electrophilic or nucleophilic molecules, and thus MEP is commonly used as a reactivity map [58]. To predict regions of electrophiles or nucleophiles, the electrostatic potential was calculated at the B3LYP/6-31G (d, p) and is shown in Figure 7. The importance of total electron density surface mapped with the electrostatic potential provides details on molecular size, shape, as well as positive or negative electrostatic potential regions in terms of color grading and this idea plays a key role in the research of molecular structure with is property relationships [59].

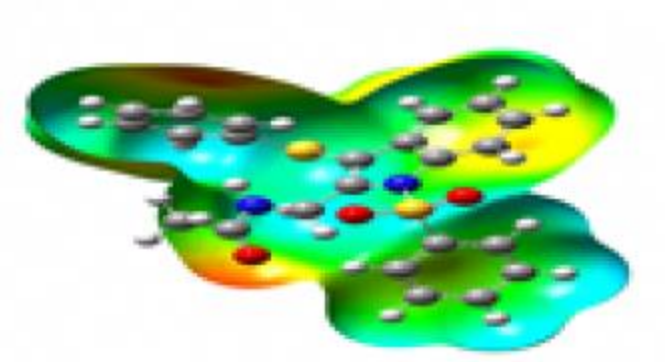

Figure 7: Molecular electrostatic potential of N-((1-(phenylsulfonyl)-3-(phenylthio)-1H-indol-2-yl)methyl)acetamide

The different values of the electrostatic potential are represented by different colors. It is accepted that the negative (red) and the positive (blue) potential regions in the mapped MEP represent regions susceptible to approach electrophiles and nucleophiles, respectively. Moreover, the MEP's contour map is used to find the ligand's regions which are more prone to incoming electrophilic species. Spatial regions denser in MEP's contour lines present stronger electrostatic fields than the region with less contour lines. In general, the red regions pictured in the total electron density surface mapped with the MEP indicate the occurrence of inward electrostatic fields, which favor the approach of electrophilic species and repel nucleophilic ones. It can be seen that the most possible sites for nucleophilic attack is H_{14} and C_{11}. Negative regions in the studied molecule are found around the O_{12}, O_{15} and O_{17} atoms indicating a possible site for electrophilic attack.

According to these calculated results, the MESP map shows that the negative potential sites are on electronegative atoms whereas the positive potential sites are around the hydrogen and carbon atoms. The contour map shown in Figure 8 provides a simple way to predict how different geometries could interact with each other.

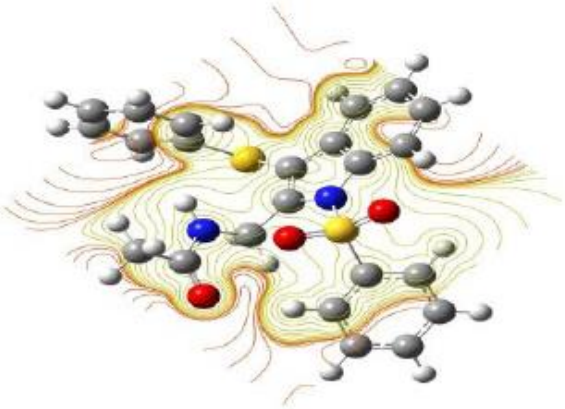

Figure 8: The contour map of electrostatic potential of the total density of N-((1-(phenylsulfonyl)-3-(phenylthio)-1H-indol-2-yl)methyl)acetamide

NBO analysis

NBO analyses provides an efficient method for studying intra and inter molecular bonding and interaction among bonds and also provides a convenient basis for investigation charge transfer or conjugative interactions in the molecular system The NBO analysis involves a sequential transformation of non-orthogonal atomic orbitals to the complete orthonormal sets of natural atomic orbitals, hybrid orbitals and bonding orbitals. These localized basis sets describe electron density and other properties by the smallest number of filled orbitals in the most rapidly convergent fashion. NBO analysis has been performed on N1P3P1HI2MA in order to elucidate many-electron molecular wave function in terms of localized electron-pair bonding units. The NBO method was one of the powerful and popular methods for the study of bonding concepts.

The NBO localization protocol divides NBOs into core, bonding, antibonding and remaining (Rydberg) orbitals. By the use of the second-order bond-antibond (donor-acceptor) NBO energetic analysis, insight on the most important delocalization schemes were obtained. The change in Electron Density (ED) in the (σ^*, π^*) antibonding orbitals and E(2) energies have been calculated by NBO analysis [60] using DFT methods to give a clear evidence of stabilization originating from various molecular interactions. The hyper conjugative interaction energy was deduced from the second-order perturbation approach [61-64].

$$E(2)= -n_{\sigma} (\sigma| F| \sigma)^2/\varepsilon$$
$$\sigma'-\varepsilon\ \sigma= F_{ij}^{\ 2}/\Delta E$$

Where, $(\sigma| F| \sigma)^2$ or $F_{ij}^{\ 2}$ is the Fock matrix element between the i and j NBOs, $\varepsilon\ \sigma'$ and $\varepsilon\ \sigma$ are the energies of σ and σ^* NBOs, and n_{σ} is the population of the donor σ orbital.

In Table 6, the significant donor–acceptor interactions and the corresponding perturbation energy values are presented. The larger the E(2) value, the intensive is the interaction between electron donors and electron acceptors. In N1P3P1HI2MA, the interactions between the antibonding C_{20}-C_{22} and the antibonding of C_{25}-C_{24} have the highest E(2) value around 238.89 kcal/mol. The other significant interactions giving stronger stabilization energy value of 235.65 kcal/mol to the structure represents the interactions between antibonding of C_{20}-C_{22} and C_{22}-C_{23}.

Table 6: NBO analysis of N1P3P1HI2MA, second order perturbation theory analysis of Fock matrix in NBO analysis

Donor(i)	Acceptor (j)	E(2)[a] (kJ/mol)	E(j)–E(i)[b] (a.u.)	F(i, j)[c] (a.u.)
π^* C_2–C_3	π^* C_4–C_9	71.58	0.05	0.081
π^* C_4–C_9	π^* C_5–C_6	191.26	0.03	0.094
π^* C_7–C_8	π^* C_5–C_6	116.75	0.03	0.087
π^* C_{11}–C_{12}	π^* C_{13}–C_{14}	122.84	0.02	0.079
π^* C_{11}–C_{12}	π^* C_{15}–C_{16}	122.73	0.02	0.077
π^* C_{20}–C_{21}	π^* C_{22}–C_{23}	235.65	0.02	0.091
π^* C_{20}–C_{21}	π^* C_{24}–C_{25}	238.89	0.01	0.083
LP(2)N1	π^* C_4–C_9	78.62	0.23	0.123
LP(1)N27	π^* C_{28}–O_{30}	58.69	0.29	0.117

Thermodynamic properties

On the basis of vibrational analysis at B3LYP/6-31G (d, p) and B3LYP/6-311++G (d, p) levels, the standard statistical thermodynamic functions: heat capacity (C) entropy (S) and enthalpy changes (ΔH) for the compound N1P3P1HI2MA were obtained from the theoretical harmonic frequencies and are listed in Table 7.

Table 7: Thermodynamic properties of N1P3P1HI2MA

T (K)	S (J/mol.K)		Cp (J/mol.K)		ddH (kJ/mol)	
	6-31 G (d, p)	6-311++G (d, p)	6-31 G (d, p)	6-311++G (d, p)	6-31 G (d, p)	6-311++G (d, p)
100	459.94	430.41	184.63	171.58	11.57	10.82
200	625.8	598.17	309.48	298.41	36.21	33.03
298.15	773.36	729.46	438.45	404.88	72.91	69.46
300	776.08	740.34	440.86	416.67	73.72	70.10
400	920.19	895.25	564.19	538.38	124.11	119.88
500	1057.62	1044.02	667.89	615.63	185.89	183.22
600	1187.05	1157.96	751.25	727.87	257.01	238.59
700	1308.05	1290.99	818.08	797.83	335.59	314.61

As observed from the Table 7, the values of C_P, H and S all increase with the increase of temperature from 100 to 1000 K, which is attributed to the enhancement of the molecular vibration as the temperature increases [65]. The variation of heat capacity, entropy and enthalpy with temperature is represented in Figure 9. The quadratic fitting of the variation of heat capacity, entropy and enthalpy with temperature is as follows.

$$C=2.98782+0.21311\ T-1.2085 \times 10^{-4}\ T^2\ (R^2=0.99991)$$
$$S=54.80821+0.52115\ T-9.1265\times 10^{-5}\ T^2\ (R^2=0.99988)$$
$$\Delta H= -0.67053+0.01478\ T-6.9612 \times 10^{-5}\ T^2\ (R^2=0.99991)$$

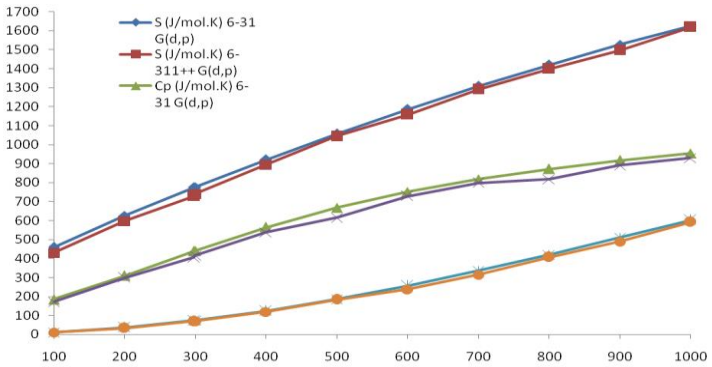

Figure 9: Thermodynamical properties of N-((1-(phenylsulfonyl)-3-(phenylthio)-1H-indol-2-yl) methyl) acetamide by B3LYP/6-31G(d,p) and B3LYP/6-311++G(d,p) method

All the thermodynamic data provide helpful information for further study on the N1P3P1HI2MA. They can be used to compute the other thermodynamic energies in the thermo chemical field [66].

CONCLUSION

The structure, molecular properties and other properties are discussed by combining spectroscopic, Density functional theory and theoretical quantum computation of atoms in molecules. Attempts have been made to ascertain the vibrational band assignments using theoretical FTIR and FT-Raman spectra, which are supported by theoretically calculated wave numbers. The nucleophilic and electrophilic sites on the molecular electrostatic potential were determined. In addition, the HOMO-LUMO property has been used to explain electronic properties. The natural bonding orbital result reflects the charge transfer in the molecule. Thus, the present investigation provides complete vibrational assignments, structural information and electronic properties of the compounds chosen.

REFERENCES

[1] U.P. Singh, B.K. Sarma, P.K. Mishra, A.B. Ray, *Folia Microbiol*., **2000**, 45, 173-176.
[2] A. Andreani, M. Granaiola, A. Leoni, A. Locatelli, R. Morigi, M. Rambaldi, G. Giorgi, L. Salvini, V. Garaliene, *Anticancer Drug Des*., **2001**, 16, 167-174.
[3] J. Quetin-Leclercq, *J. Pharm. Belg*., **1994**, 49, 181-192.
[4] S. Mukhopadhyay, G.A. Handy, S. Funayama, G.A. Cordell, *J. Nat. Prod*., **1981**, 44, 696-700.
[5] D.L. Taylor, P.S. Ahmed, P. Chambers, A.S. Tyms, J. Bedard, J. Duchaine, G. Falardeau, J.F. Lavallee, W. Brown, R.F. Rando, T. Bowlin, *Antiviral Chem. Chemother*., **1999**, 10, 79-86.
[6] T.M. Williams, T.M. Ciccarone, S.C. MacTough, C.S. Rooney, S.K. Balani, J.H. Condra, E.A. Emini, M.E. Goldman, W.J. Greenlee, L.R. Kauffman, *J. Med. Chem*., **1993**, 36, 1291-1294.
[7] J. Sivaraman, K. Subramanian, D. Velmurugan, E. Subramanian, J. Seetharaman, *J. Mol. Struct*., **1996**, 385, 123-128.
[8] S. Thenmozhi, A. SubbiahPandi, V. Dhayalan, A.K. MohanaKrishnan, *Acta Cryst*., **2009**, E65, o1020-o1021.
[9] M.J. Frisch, Gaussian, Inc: Wallingford CT, **2009**, 9.
[10] M. Govindarajan, K. Ganasan, S. Periandy, M. Karabacak, *Spectrochim. Acta A*., **2011**, 79, 646
[11] S. Cradock, C. Purves, D.W.H. Rankin, *J. Mol. Struct*., **1990**, 220, 193.
[12] Z. Zhengyu, D.U. Dongmei, *J. Mol. Struct*., **2000**, 505, 247.
[13] Z. Zhengyu, F.U. Aiping, D.U. Dongmei, *Int. J. Quant. Chem*., **2000**, 78, 186.
[14] W. Kohn, L.J. Sham, *Phys. Rev*., **1965**, 140, A1133-A1138.
[15] A.D. Becke, *J. Chem. Phys*., **1993**, 98, 5648-5652.
[16] C. Lee, W. Yang, R.G. Parr, *Phys. Rev*., **1988**, B37, 785-789.
[17] B. Miehlich, A. Savin, H. Stoll, H. Preuss, *Chem. Phys. Lett*., **1989**, 157, 200-206.
[18] A.P. Scott, L. Random, *J. Phys. Chem*., **1996**, 100, 16502-16513.
[19] P. Pulay, G. Fogarasi, G. Pongor, J.E. Boggs, A. Vargha, *J. Am. Chem. Soc*., **1983**, 105, 7037-7047.
[20] A.E. Frisch, H.P. Hratchian, I.I.R.D. Dennington, T.A. Keith, John Millam, A.B. Nielsen, A.J. Holder, J. Hiscocks, Gaussian, Inc: Gauss View Version 5.0., **2009**.
[21] M.H. Jamroz, Vibrational Energy Distribution Analysis: VEDA 4 Program Warsaw, Poland, **2004**.
[22] G. Keresztury, S. Holly, J. Varga, G. Besenyei, A.Y. Wang, J.R. Durig, *Spectrochim. Acta A*., **1993**, 49, 2007-2017.
[23] G. Keresztury, In Raman Spectroscopy: Theory-Handbook of Vibrational Spectroscopy, Editors-J.M. Chalmers, P.R. Griffith, John Wiley & Sons, New York., **2002**.
[24] www.sigmaaldrich.com.
[25] E.D. Glendening, A.E. Reed, J.E. Carpenter, F. Weinhold, University of Wisconsin, Madison, **1998**.
[26] A.D. Buckingham, *Adv. Chem. Phys*., **1967**, 12, 107-142.
[27] D.R. Kanis, M.A. Ratner, T.J. Marks, *Chem. Rev*., **1994**, 94, 195-242.
[28] J.A. Pople, H.B. Schlegel, R. Krishnan, D.J. Defrees, J.S. Binkley, M.J. Frisch, R.A. Whiteside, R.F. Hout, W.J. Hehre, *Int. J. Quantum Chem*., **1981**, 15, 269-278.
[29] S. Gunasekaran, S. Seshadri, S. Muthu, S. Kumaresan, R. Arunbalaji, *Spectrochim. Acta A*., **2008**, 70, 550-556.
[30] N. Puviarasan, V. Arjunan, S. Mohan, *Turk. J. Chem*., **2002**, 26 323-334.
[31] G. Varsanyi, Vibrational Spectra of Benzene Derivatives, Academic Press, NY, USA, **1969**.
[32] V. Krishnakumar, R. John Xavier, *Indian J. Pure Appl. Phys*., **2003**, 41, 597-602.

[33] V. Krishnakumar, V.N. Prabavathi, *Spectrochim. Acta A.*, **2008**, 71, 449-457.
[34] A. Altun, K. Golcuk, M. Kumru, *J. Mol. Struct*., **2003**, 637, 155-169.
[35] G. Socrates, Infrared Characteristic Group Frequencies, John Wiley, New York., **2000**.
[36] N. Puviarasan, V. Arjunan, S. Mohan, *Turk.J. Chem.*, **2002**, 26,323.
[37] R.M. Silverstein, C.G. Bassler, C.T. Morill, John Wiley, NY, USA, **1997**.
[38] S. Gunasekaran, S.R. Varadhan, K. Manoharan, *Asian J. Phys*., **1993**, 12.
[39] S. Mohan, S. Gunasekaran, S.Salainathan, *Acta Ciencia India*., **1998**, 15, 77.
[40] J. Umemura, S. Hayashi, *Bull. Inst. Chem. Res. Kyoto Univ*., **1974**, 52, 585.
[41] P. Venkataramana Rao, G. Ramana Rao, *Spectrochim. Acta Part A.*, **2002**, 58(14), 3205.
[42] D.K. Jain, V. Jain, G.N. Singh, M.K. Sonawame, *Asian J. Phys*., **2000**, 9(2), 487-489.
[43] P. Venkataramana Rao, G. Ramana Rao, *Spectrochim Acta Part A.*, **2003**, 59, 637.
[44] S. Seshadri, S. Gunasekaran, S. Muthu, *J. Raman Spec*., **2009**, 40, 639-644.
[45] M. Govindarajan, M. Karabacak, *Spectrochim. Acta Mol. Biomol. Spectrosc*., **2012**, 96, 421-435.
[46] P. Govindasamy, S. Gunasekaran, S. Srinivasan, *Spectrochim. Acta Mol. Biomol. Spectrosc*., **2014**, 130, 329-336.
[47] N.M. O' Boyle, A.L. Tenderholt, K.M. Langer, *J. Comput. Chem*., **2008**, 29, 839-845.
[48] R.G. Parr, L. Szentpaly, S. Liu, *J. Am. Chem. Soc*., **1999**, 121, 1922-1924.
[49] I. Fleming, Frontier Orbitals and Organic Chemical Reactions Wiley, London., **1976**.
[50] A.Y. Musa, A.H. Kadhum, A.B. Mohamad, Rohoma, H. Mesmari, *J. Mol. Struct.*, **2010**, 969, 233.
[51] B. Kosar, C. Albayrak, *Spectrochim Acta A.*, **2010**, 78, 160-167.
[52] N.O. Obi-Egbedi, I.B. Obot, M.I. El-Khaiary, *J. Mol. Struct*., **2011**, 1002, 86-96.
[53] T.C. Koopmans, *Physica (Amsterdam)*., **1933**, 1, 104.
[54] E.E. Ebenso, T. Arslan, F. Kandemirli, I. Love, C. Og˘retir, M. Saracog˘lu, S.A. Umoren, *Int. J. Quantum Chem*., **2010**, 110, 2614.
[55] R. Parthasarathi, J. Padmanabhan, M. Elango, V. Subramanian, P. Chattaraj, *Chem. Phys. Lett*., **2004**, 394, 225-230.
[56] R. Parthasarathi, J. Padmanabhan, V. Subramanian, B. Maiti, P. Chattaraj, *Curr. Sci*., **2004**, 86, 535-542.
[57] R. Parthasarathi, J. Padmanabhan, V. Subramanian, U. Sarkar, B. Maiti, P. Chattaraj, *Internet Electron. J. Mol. Des*., **2003**, 2, 798-813.
[58] M. Govindarajan, M. Karabacak, S. Periandy, S. Xavier, *Spectrochim. Acta Mol. Biomol. Spectrosc*, **2012**, 94, 53-64.
[59] C. Munoz-Caro, A. Niño, M.L. Senent, J.M. Leal, S. Ibeas, *J. Org. Chem*., **2000**, 65, 405-410.
[60] H.W. Thomson, P.J. Torkington, *J. Chem. Soc*., **1945**, 171, 640-646.
[61] E.D. Glendening, J.K. Badenhoop, A.E. Reed, J.E. Carpenter, J.A. Bohmann, C.M. Morales, F. Weinhold, Theoretical Chemistry Institute, University of Wisconsin, Madison., **2001**.
[62] A.E. Reed, F. Curtiss, F. Weinhold, *Chem. Rev*., **1988**, 88, 899-926.
[63] A.E. Reed, P.V.R. Schleye, *Inorg. Chem*., **1988**, 27, 3969-3987.
[64] R.J. Xavier, E. Gobinath, *Spectrochim. Acta A.*, **2012**, 91, 248-255.
[65] J. Bevan Ott, Academic Press., **2000**.
[66] R. Zhang, B. Dub, G. Sun, Y. Sun, *Spectrochim. Acta A*., **2010**, 75, 1115.